Atmos. Meas. Tech. Discuss., 8, 13331–13375, 2015
www.atmos-meas-tech-discuss.net/8/13331/2015/
doi:10.5194/amtd-8-13331-2015

Atmospheric Measurement Techniques Discussions

Industrial SO_2 emissions monitoring using a portable multi-channel gas analyzer with an optimized retrieval algorithm

Y. W. Sun[1,*], C. Liu[2,1,*], P. H. Xie[1,2], A. Hartl[3], K. L. Chan[4], Y. Tian[1], W. Wang[1], M. Qin[1], J. G. Liu[1,2], and W. Q. Liu[1,2]

[1]Key Lab of Environmental Optics & Technology, Anhui Institute of Optics and Fine Mechanics, Chinese Academy of Sciences, Hefei 230031, China
[2]University of Science and Technology of China, Hefei, 230026, China
[3]School of Energy and Environment, City University of Hong Kong, Hong Kong, China
[4]Meteorological Institute, Ludwig-Maximilians Universität München, Munich, Germany
[*]These two authors contributed equally to this work.

Received: 21 July 2015 – Accepted: 2 December 2015 – Published: 17 December 2015

Correspondence to: C. Liu (chliu81@ustc.edu.cn) and Y. W. Sun (ywsun@aiofm.ac.cn)

Published by Copernicus Publications on behalf of the European Geosciences Union.

Abstract

In this paper, we demonstrate achieving accurate industrial SO_2 emissions monitoring using a portable multi-channel gas analyzer with an optimized retrieval algorithm. The introduced analyzer features with large dynamic measurement range and correction of interferences from other co-existing infrared absorbers, e.g., NO, CO, CO_2, NO_2, CH_4, HC, N_2O and H_2O. Both effects have been the major limitations of industrial SO_2 emissions monitoring. The multi-channel gas analyzer measures 11 different wavelength channels simultaneously in order to achieve correction of several major problems of an infrared gas analyzer, including system drift, conflict of sensitivity, interferences among different infrared absorbers and limitation of measurement range. The optimized algorithm makes use of a 3rd polynomial rather than a constant factor to quantify gas-to-gas interference. The measurement results show good performance in both linear and nonlinear range, thereby solving the problem that the conventional interference correction is restricted by the linearity of both intended and interfering channels. The result implies that the measurement range of the developed multi-channel analyzer can be extended to the nonlinear absorption region. The measurement range and accuracy are evaluated by experimental laboratory calibration. An excellent agreement was achieved with a Pearson correlation coefficient (r^2) of 0.99977 with measurement range from ~ 5 ppmv to 10 000 ppmv and measurement error < 2 %. The instrument was also deployed for field measurement. Emissions from 3 different factories were measured. The emissions of these factories have been characterized with different co-existing infrared absorbers, covering a wide range of concentration levels. We compared our measurements with the commercial SO_2 analyzers. The overall good agreements are achieved.

1 Introduction

High accuracy SO_2 emissions monitoring is in great demand for the purpose of industrial process identification and pollution emissions regulation. Industrial SO_2 emis-

AMTD
8, 13331–13375, 2015

sions often varies over a large range during different production processes (Chan et al., 2008; Terje, 1996; Zu, 2002; Liu et al., 2012). For example, SO_2 emissions from a copper smelting plant are of the order of ppmv or even less when the smelting period is nearly finished, but SO_2 emissions can be up to several thousands ppmv or even higher during the smelting period. SO_2 emissions from industrial desulfurization processes (a chemical reaction process to reduce SO_2 emissions) are usually higher than 600 ppmv during the process, but lower than 200 ppmv otherwise (EPER, 2004; European Commission, 2007; Evans et al., 2009). It's impossible to measure accurately the SO_2 concentrations varying in such a huge range with single absorption band analyzer due to the conflict of sensitivity and limitation of measurement range (Andre et al., 1985; Dirk et al., 2009). Furthermore, stack emissions also consist of many other infrared absorbing gases such as NO, CO, CO_2, NO_2, N_2O, HC, CH_4 and H_2O. All these gases may interfere with each others (Andre et al., 1985; Dirk et al., 2009). To measure SO_2 emissions with high accuracy, cross interferences have to be corrected. In general, a commercial multi-gas analyzer, e.g., Model 60i made by Thermo Fisher Scientific or Li-7500 made by Li-cor, specifies a particular application where both the intended and interfering channels lie within linear ranges. Thus, cross interference can be corrected by using the conventional look-up table (consists of various constant factors to quantify gas-to-gas interferences) approach (Herget et al., 1976; Jacob et al., 2012; Dirk et al., 2009; Harold et al., 1993). In this case, SO_2 concentrations within a certain linear range can be well resolved. However, the conventional interference correction introduces large uncertainty due to nonlinear absorption when the intended or interfering gases concentration lies beyond a threshold (Sun et al., 2013). In cases the conventional correction of cross interferences is not possible, one has to resort to other methods. For example, one can expand the linear range to higher concentrations by reducing the optical path length or selecting a relatively weak absorption waveband. However, both approaches have considerable disadvantages (Mark et al., 1983; Mauri et al., 2001). Reducing the optical path length will also influence the whole measurement system. Sensitivity and measurement range of other gases will also be dete-

AMTD
8, 13331–13375, 2015

riorated. Selecting a relatively weaker absorption waveband for a certain gas would reduce the sensitivity to this gas for all applications (Lambrecht, 2005; Gary, 2002). Sun et al. (2013) proposed a new cross interference correction technique which works well even when nonlinear absorption occurs (Sun et al., 2013). Consequently, the measurement range of a multi-channel analyzer can be extended by a factor of about $2 \sim 4$. However, in some extreme cases, saturated absorption[1] occurs and the new technique also fails.

In this paper, we propose to solve all above conflicts by measuring SO_2 emissions using a multi-channel gas analyzer with an optimized retrieval algorithm. This paper is an extended study of Sun et al. (2013) but many optimizations both in instrumentation and retrieval algorithm are performed. Mainly:

- To avoid the saturated absorption of SO_2, we introduce two channels for SO_2 measurements. One of the absorption channel which lies on a relative strong SO_2 absorption band measures SO_2 in the lower concentration range, another absorption channel which lies on a weaker absorption band measures SO_2 in the higher concentration range. As a result, a good balance between sensitivity and measurement range can be obtained.

- The number of the analysis channel is expanded from 8 to 11. More interfering gases are taken into account and the system is thus robust in various industrial SO_2 emissions measurements.

- In Sun et al. (2013), the interference equations are set up depend on interference conditions. The gas to gas interference is represented by a conventional constant factor if no nonlinear absorption happens, while it is represented by a 3rd polynomial if nonlinear absorption happens. Besides, the H_2O interference correction is included in the interference equations. In this study, all gas to gas interferences

[1]The absorbance no longer vary with gas concentrations because of concentrations beyond the upper limit of a channel.

AMTD
8, 13331–13375, 2015

are represented by 3rd polynomials. The H_2O interference is corrected in a separate way which shortens the calculation time when solving the interference equations. The optimized manner makes the system robust in both linear and nonlinear conditions. And thus can be easier adapted for other applications.

As a result, the optimized algorithm greatly improved the linearity restriction of interference correction of both intended and interfering channels. Furthermore, it greatly improved the measurement range by solving the saturated absorption problem and expanding accurate interference correction from linear absorption region to nonlinear absorption region.

In contrast to other well established spectroscopic gas analyzer, e.g., DOAS (differential optical absorption spectroscopy) analyzer or FTIR (Fourier transform infrared spectroscopy) analyzer, etc., the developed measurement technique presented here has advantages of a simple set up, a wide measurement range for multi-gas analysis at low cost and with good durability. Furthermore, It is more robust compared to a commercial multi-gas analyzer.

2 Instrument description

All experiments are performed with the compact multi-channel gas analyzer prototype. The weight of the entire system is about 5 kg. Figure 1 shows the functional structure of this instrument. The light source (a globar) can be represented by a blackbody with a temperature of 1200 K (927 °C) covering infrared wavebands between 1 to 10 µm and with a maximum radiation wavelength λ_{max} at 2.42 µm. Incoming light is reflected several times between three spherical mirrors (f = 396.3 mm) to increase the light path length when it passes through the sample gas (resulting in 12 m optical path length within a 60 cm long White cell). The sample cell is kept at 343 K (50 °C) by using a temperature controller. The advantage of this prototype compared to a commercial gas analyzer is that it has a replaceable filter wheel which can be exchanged for other measurement. Suitable filter combinations allow measuring a variety of gases,

AMTD
8, 13331–13375, 2015

such as SO_2, NO_2, CH_4, N_2O, HC, H_2O, CO_2, CO, NO and NO_2, etc. simultaneously (Sun et al., 2013). Our setup consists of 4 different filter wheels, a 4-channels filter wheel for atmospheric CO_2 and H_2O measurements, a 5-channels filter wheel for farmland/grassland/wetland CO_2 and CH_4 flux measurements and a 8 or 11-channels filter wheel for industrial emissions measurement. The corresponding signal sampling interval and data processing scenario can be adjusted according to the combination of filters.

For industrial emissions measurements, it's the 8 or 11-channels filter wheel will be selected depends on the interfering gases type in the emissions. The filter wheel used in this study has 11 filter channels. Simultaneous measurement in 11 different wavelength channels is realized by used 11 different band pass filters. One channel is used for system drift correction, two channels for SO_2 measurement, and the other 8 channels are used to correct the interferences from NO, CO, CO_2, NO_2, CH_4, HC, N_2O and H_2O.

3 Filter parameters calculation

We determine the filter parameters for all channels based on the measurement range requirements. We assume that the instrument can reliably resolve optical signal attenuation between 5 and 95 % (an empirically estimated range based on the response performance of the detector), i.e. the response range of the instrument lies between $I_S = 0.05I_0$ and $I_S = 0.95I_0$. Then it follows from Lambert–Beer's law that the resolved absorbance range lays between 0.05129 and 2.9957. The optical path length is a known constant (L = 1200 cm), so the measurement range of the instrument can be estimated once α is derived. Here I_0 and I_S represent incident and emergent intensity, respectively. Both of which can be obtained by the detector. α ($cm^2\,molec^{-1}$) is the total absorption coefficient of a gas within a specified wavelength interval $\Delta\lambda$, which can be calculated by a line-by-line integration method (Sparks, 1997; Martin et al., 1998; Rothman et al., 2005, 2009).

AMTD
8, 13331–13375, 2015

The absorption spectra of SO_2 between 2 and 10 µm obtained from the HITRAN database are shown in Fig. 2. There are three obvious absorption wavebands within this region: at 4, 7.32 and 8.5 µm. The line strengths of these three wavebands can be ranked as 7.32 µm > 8.5 µm > 4 µm with values 10^{-19}, 10^{-20} and 10^{-21} cm molecule^{-1}, respectively. Considering the radiation spectrum of the light source (the blue solid curve in Fig. 2), we select the 7.32 and 4 µm wavebands to measure low and high concentration levels of SO_2 for a wide range from several ppmv to more than 10 000 ppmv. The 3.73 µm band where SO_2 and the interference gases NO, CO, CO_2, NO_2, CH_4, HC, N_2O and H_2O show no or negligible absorption is selected as the reference channel. Once the center wavelength of each filter channel is selected, its bandwidth can be determined using the following iterative scheme (Ehret et al., 1993; Bingham et al., 1984).

1. Choose a starting wavelength interval $\Delta\lambda$ with a small value, set T to the temperature of the sample cell and P to one standard atmospheric pressure, i.e. $T = 343$ K and $P = 101\,325$ Pa. Each line within this wavelength interval is described by a Voigt profile together with the pressure and temperature dependence of the absorption line strengths and half-widths (Rothman et al., 2005, 2009). Thus, total absorption coefficients of SO_2 at the three filter channels can be calculated numerically by a line-by-line integration (Sparks, 1997; Martin et al., 1998). The measurement range of each filter channel can then be estimated from this total absorption coefficient and the abovementioned absorbance range. Note that, to simplify the line-by-line calculation, the uneven distribution of the light source and the response function of the detector within a specified interval are neglected. Furthermore, the transmission function $t(\lambda)$ of a selected filter is approximated as a Gaussian function with maximum transmission of 75 %. In this case, $t(\lambda)$ can be expressed as

$$t(\lambda) = \exp\left(-\left(\frac{\lambda - \lambda_0}{\Delta\lambda/4}\right)^2\right) \quad (1)$$

AMTD
8, 13331–13375, 2015

where λ_0 represents center wavelength. Here $\Delta\lambda/4$ rather than the half-width of $\Delta\lambda/2$ is used because calculation results show that a Gaussian function of this form is closer to the actual transmission function of our filter (see Sect. 5.2).

2. If the measurement range estimated in step 1 meets the requirement, the iteration is stopped and the bandwidth of this filter is determined. Otherwise, increase $\Delta\lambda$ by a small step Δ and return to step 1 to calculate the next parameters.

Two important aspects should be considered for this iteration process:

a. The determination of all filter parameters should take into account the radiation distribution of the light source at each filter channel (see Fig. 2). The bandwidth of a waveband near the maximum radiation wavelength λ_{max} should be narrower than the one of a waveband further away from it. Filters are designed accordingly in a manner that ensures the optical signals of all channels are detected with the same precision under zero gas condition (e.g., 99.999 % N_2). Therefore, the bandwidth of the 7.32 µm (SO_2 (L)) waveband should be wider than the 4 µm (SO_2 (H)) and 3.73 µm (Ref) waveband.

b. The narrower the reference filter channel, the less interference from other gases, and the better the system. However, it should be ensured that the optical signal of the reference filter channel fulfills aspect (a).

Parameters of the SO_2 (L), SO_2 (H) and reference filter determined as aforementioned method are listed in Table 1. The corresponding calculation results are contained in Table 2. Parameters of all other 8 filters are obtained in a straightforward manner. Table 2 shows that the total absorption coefficient of SO_2 for the reference channel relative to the SO_2 (L) and SO_2 (H) channel is only 6.1×10^{-5} and 2.76×10^{-3}, respectively. The lower detection limit of the reference channel for SO_2 is 88270.9 ppmv, which means that signal attenuation for this channel caused by SO_2 absorption (with concentration lower than 10 000 ppmv) can be neglected. Therefore temporal variations of this channel are only caused by system drifts and the reference channel can indeed be used to

AMTD
8, 13331–13375, 2015

correct the other channels (Jacob et al., 2012; Sun et al., 2013). The total absorption coefficient of SO_2 for the SO_2 (H) channel is only 2.02 % of the SO_2 (L) channel. If SO_2 is measured only using the SO_2 (L) channel, a good lower detection limit of 5.37 ppmv can be obtained. However, its top detection limit is only 313.904 ppmv due to the strong absorption. The top detection limit of the SO_2 (H) channel is up to 14224.6 ppmv. However, its lower detection limit is only 243.56 ppmv. Combining both SO_2 (L) and SO_2 (H) channels allows measuring low and high concentrations of SO_2 from several ppmv to at least 10 000 ppmv. As a result, the saturated absorption of SO_2 is avoided and measurement range are improved significantly.

4 Optimized concentration retrieval algorithm

Without correcting cross-sensitivities caused by interfering gases, a gas analyzer is still not capable to resolve industrial SO_2 emissions over a wide range of variation even if two absorption channels are used. The conventional method is only feasible for an application where both the intended and interfering channels exhibit good linearity. In the following, we present an optimized SO_2 concentration retrieval algorithm to make the instrument work well within both the linear and nonlinear range.

Briefly, the optimized SO_2 concentration retrieval is illustrated in Fig. 3. The retrieval algorithm (1) converts measurements values of all relevant channels into absorbance, (2) corrects for water vapor interference using the H_2O channel, (3) makes cross interference corrections using interference equations, and (4) finally converts the cross interference corrected absorbance values into SO_2 concentrations. The nomenclature in Fig. 3 is listed in Table 3. We use an interference function rather than a constant factor to quantify gas-to-gas interference. All interference functions used in this study can be obtained by least-squares fits a 3rd polynomial (Sun et al., 2013). We now go through the steps on Fig. 3 in more detail.

1. Intensities of all other ten analysis channels are divided by the reference channel to correct for hardware instability, the intensities are then converted to ab-

AMTD
8, 13331–13375, 2015

sorbance. This step produces drift compensated absorbance representing the total absorption for each channel.

2. The H_2O channel used for water vapor interference correction is designed to have a center wavelength of 2.59 µm and bandwidth of 0.064 µm. Total absorption coefficients calculated as in Sect. 3 show that the H_2O channel has negligible response to other gases. Thus, water vapor interference can be corrected in this easy way. In fact, (2) can be merged with (3), resulting in 10 instead of 9 interference equations that have to be solved simultaneously. The separation of the H_2O channel proposed here facilitates the interference equations to be solved and then speeds up the concentration retrieval. This step produces water vapor interference corrected absorbance, which represent total absorption of each channel with H_2O absorption subtracted.

3. A set of interference equations is set up using all fitted interference functions and the water vapor interference corrected absorbance acquired in (2). Solution of this system of equations yields pure absorbance for each gas. Since absorbance are additive, the data processor can solve these equations iteratively. In detail: the data processor sets up nine interference equations and creates a loop which will "solve" these equations multiple times. The data processor starts the loop with the absorbance corrected for water vapor interference and uses the output of the loop as input for the next iteration. Taking the first equation (for SO_2) as an example, the data processor assumes that the total absorbance is generated by SO_2 (disregarding interferences) and the absorbance of other gases are zero. With each pass through the loop, the data processor obtains new absorbance that will then be available for the next iteration. In the second iteration, the data processor now has estimated absorbance for each gas, so it can apply the fitted interference functions and calculate the amount of interference that each gas would create in every channel. This will only be a rough approximation, but with each pass through the loop, the estimate gets better and finally produces cross

AMTD
8, 13331–13375, 2015

interferences corrected absorbance, which represent pure absorptions for each gas.

4. The pure absorbance calculated in step (1)–(3) are now used for concentration retrieval with corresponding calibration curves. Flow chart of SO_2 retrieval is shown in Fig. 4. The concentration retrieval is attributed to the SO_2 (L) channel if the absorbance of this channel is lower than 1.5, otherwise it is assigned to the SO_2 (H) channel. Calibration curves with four zero and/or span factors are used if the instrument has been zero and/or span calibrated. Otherwise, the default calibration curves are applied. The calibration curves fitting is given in Sect. 5.1.

5 Laboratory experiments and discussion

5.1 Calibration curves fitting

Calibration curves of both SO_2 (L) and SO_2 (H) can be obtained by assuming a parameterized (model) form of the concentration-absorbance relationship. The model parameters are determined from least-squares fit to measured concentrations (Komhyr et al., 1983, 1989; Bjorck, 1996; Rao et al., 1999; Derek, 1968; Marcel et al., 1990). There are in principle two different well-established fit models to determine the calibration curves, the linear function and polynomial. In general, a gas analyzer has a good linearity if gas concentrations lie within a specified range. In this case, a linear function model is used. Otherwise, a polynomial model is applied to obtain a relatively wider measurement range. Because a polynomial can effectively model nonlinear absorption of a system compared with a linear function (Andre et al., 1985; Tan et al., 2008). Here, a 3rd order polynomial model is used. The calibration experiments were carried out as following. Different concentration levels of SO_2 generated by a gas generator were pumped into the sample cell. Each selected SO_2 level was stably maintained in the sample cell for the duration of five times the response time of the instrument to guarantee accurate optical intensity acquisitions. The data processor converts intensities at

AMTD
8, 13331–13375, 2015

the SO_2 (L) and SO_2 (H) channels into absorbance. The resulting data array (τ_i^X, C_i) for $i = 1 \sim n$ concentration values C_i and corresponding average absorbance values τ_i^X of both channels $X = SO_2$ (L), SO_2 (H) provide the input for calibration fit. SO_2 concentrations below 280 ppmv are attributed to the SO_2 (L) channel, while concentrations $\geq$ 280 ppmv are assigned to SO_2 (H) channel. We selected the concentration value of 280 ppmv to separate the channels SO_2 (L) and SO_2 (H) because this way we found a good balance between accuracy and linearity. The boundary value 280 ppmv is an empirical result of multiple experiments. Figures 5a and b show the fitted calibration curves of the SO_2 (L) and SO_2 (H) channels, respectively. The fit parameters and their estimated errors, as well as Pearson correlation coefficients are included in both subfigures. Figure 5 shows that both SO_2 (L) and SO_2 (H) channels exhibit excellent fit results, with correlation coefficients of 0.9999 and 0.9998, respectively. The calibration curves of the two channels are expressed as Eqs. (2) and (3), respectively.

$$f_{SO_2(L)}(\tau) = 5.40386 + 94.58219 \cdot \tau + 44.59494 \cdot \tau^2 + 11.43462 \cdot \tau^3 \quad (2)$$

$$f_{SO_2(H)}(\tau) = -109.98492 + 4402.11471 \cdot \tau + 229.94456 \cdot \tau^2 + 406.11472 \cdot \tau^3 \quad (3)$$

Generally, calibration curves change with time due to instrument drift. Thus, zero and span calibrations have to be carried out and taken into account in the model for the calibration curve. This can be achieved by introducing zero and span factors, so that the actual calibration curves of SO_2 (L) and SO_2 (H) become

$$f^{cal.}_{SO_2(L)}(\tau) = d_0 \times f_{SO_2(L)}(\tau) + j_0 \quad (4)$$

$$f^{cal.}_{SO_2(H)}(\tau) = d_1 \times f_{SO_2(H)}(\tau) + j_1 \quad (5)$$

where j_0 and d_0 denote zero and span factors for the SO_2 (L) channel and j_1 and d_1 denote zero and span factors for SO_2 (H) channel. These correction factors are again obtained from measurements with calibration gases. We performed Allan variance analysis to the measurement result, a compromise calibration cycle of 25 days is obtained for both SO_2 (L) and SO_2 (H) channels (Jacob et al., 2012; Sun et al., 2013).

AMTD
8, 13331–13375, 2015

5.2 Evaluation of the measurement range

Since systematic errors are generally hard to quantify, commonly two approaches to estimate the detection limit are employed (Lopez and Frutos, 1993; Sayed et al., 2010; Tyson et al., 1984). The first approach uses the concentration calculated for an absorbance equal to two times the standard deviation of the absorbance (2σ absorbance) under zero gas (e.g., 99.999 % N_2) condition to define the lower detection limit. The second approach has already been mentioned in Sect. 3. It assumes that a analyzer can only resolve optical signal attenuation above a critical threshold. Converting it to absorbance and employing the corresponding calibration curve for the concentration retrieval results in an alternative definition of the lower detection limit. We compare both approaches taking 5 % signal attenuation as threshold for the second approach. Figure 6 shows an absorbance time series for the SO_2 (L) and SO_2 (H) channels under zero gas (99.999 % N_2) condition. Ten measurement cycles are averaged, resulting in a temporal resolution of about four seconds per reading. Statistical results for more than 10 h are listed in Table 4. For an 2σ absorbance, the calibration curves for the SO_2 (L) and SO_2 (H) channel give lower detection limits of 5.55 and 102.15 ppmv, respectively. In comparison, the second approach results in lower detection limits of 10.37 and 116.46 ppmv for the SO_2 (L) and SO_2 (H) channel. The top detection limits for both channels are estimated by assuming that 95 % of signal attenuation (absorbance 2.9957) represents the top limit of the analyzer. The values are and channel are 997.23 ppmv (L) and 26 059.02 ppmv (H). It can be concluded from either estimation approaches that the combination of the SO_2 (L) and SO_2 (H) channel is capable of measuring SO_2 concentrations from several ppmv to at least 10 000 ppmv, which is in good agreement with Sect. 3.

The differences between the measurement ranges estimated here and in Sect. 3 can have various reasons. Firstly, estimations in Sect. 3 and here are based on linear Lambert–Beer's Law and 3rd calibration curves (Eqs. 4 or 5), respectively, which results in different detection limits. Secondly, assumptions and approximations during

AMTD
8, 13331–13375, 2015

the numerical line-by-line integration result in errors, e.g. errors caused by the approximation of the transmission function for a filter by a Gaussian, as well as neglecting the uneven distribution of the light source and the response function of the detector within a specified region. Figure 7 shows the actual transmissions of each filter designed according to Table 1. They obviously deviate from the assumed Gaussian shape. Apart from dips in real transmissions for the reference and SO_2 (H) channel, a notable shift of the center wavelength of the SO_2 (L) channel of about 0.03um occurs. All these factors may result in differences between calculated and actual values. Thirdly, the signal attenuation assumed in the above estimations may contain a small portion of additional attenuation, e.g. attenuation due to scattering by dust, depositions on the filters, voltage fluctuations and temperature drifts of the sample cell, etc. These non-gas absorption processes are unavoidable and cannot be fully corrected by using a reference channel.

In addition to the error sources just mentioned, there is a principle problem in assuming a 95 % signal attenuation for the estimation of the top detection limit. The absorption spectrum within the full-width of a filter consists of a large number of closely spaced lines. Between these lines absorption does not occur, Lambert–Beer's Law does not apply, and, regardless of the gas concentration, the assumed 95 % attenuation of the total signal can hardly be reached in practice. For this reason we set the top detection limits of SO_2 (L) and SO_2 (H) channel as 280 and 10 000 ppmv, respectively, although the estimated values are in fact higher. Besides, for this conservative estimate of the upper detection limit, the instrument features a better linearity for SO_2.

5.3 Evaluation of the measurement accuracy

Gas mixtures (N_2, H_2O, CO_2, CO, NO_x and SO_2) with 15 spans of SO_2 are pumped sequentially into the sample cell for analysis after the instrument has been zero and span calibrated. Five and ten spans lie within the measurement range of SO_2 (L) and SO_2 (H) channel, respectively. Gas mixtures are mixed in a manner that all the H_2O, CO_2, CO, NO_x channels exhibit nonlinear absorptions at least once within all the 15 measurements. The optimized concentration retrieval algorithm are embedded and the

AMTD
8, 13331–13375, 2015

SO_2 measurement results and corresponding measurement errors are listed in Table 5. We define the absolute measurement bias $|\Delta C|$ and relative measurement error γ as Eq. (6).

$$\gamma = \frac{|\Delta C|}{C_T}$$
$$\Delta C = C_M - C_T \quad (6)$$

where C_T and C_M represent the true and measured concentration. Table 5 shows that relative measurement errors in most cases are less than 2 %. Figure 8 shows the correlation between measured concentrations and true concentrations. An excellent correlation coefficient r^2 of 0.99977 is obtained (Lopez and Frutos, 1993; Sayed et al., 2010; Tyson et al., 1984). Measurement bias and relative measurement errors are shown in Fig. 9. As for the same channel, measurement biases for low concentrations are obviously less than those for high concentrations. Possible reason is that high concentrations are relatively easier influenced by span calibration error. Furthermore, measurement biases of SO_2 (H) channel are obviously larger than those of SO_2 (L) channel. Because SO_2 (H) channel is less sensitive to signal attenuation compared with SO_2 (L) channel. Thus, system noise has relative more influence on SO_2 (H) channel than SO_2 (L) channel. However, both channels show that relative measurement errors for high concentrations are obviously less than those for low concentrations because of larger denominators to divide by (see Eq. 6).

5.4 Comparison between the conventional and optimized methods

We use different combinations of SO_2, H_2O and N_2 gases to simulate both the linear and nonlinear absorption at the H_2O channel. The SO_2 concentration was kept at a constant while H_2O concentration was filled from low to high level. This allows for a gradual variation of the H_2O channel from the linear to the nonlinear range of absorption. 243 and 6672 ppmv were respectively selected as the reference for SO_2 (L) and SO_2 (H). Figure 10 shows the comparison of relative measurement errors between

AMTD
8, 13331–13375, 2015

the conventional and the optimized retrieval algorithm. Both the conventional and the optimized methods work well if H_2O absorption lies within a linear range, and all relative measurement errors are less than 2 %. However, the optimized method works much better than the conventional one if nonlinear absorption appears. In this case, nonlinear absorption has negligible influence on the optimized method, whereas measurement errors using the conventional method deteriorated abruptly. In addition, the H_2O nonlinear absorption has more influence on SO_2 (L) channel than SO_2 (H) channel. This because H_2O exhibits stronger interference to SO_2 (L) channel than SO_2 (H).

We performed similar experiments to simulate both the linear and nonlinear absorption at other channels, the superiority of the optimized method was also concluded from the comparisons.

6 Field campaigns

The multi-channel analyzer has been used to monitor SO_2 emissions of three factories. The locations of the three factories are depicted in Fig. 11. They are located in the suburbs of Tongling city (south of Hefei, Anhui province) in central China, where they form a triangle near the Yangtze River. All the factories, i.e., Fuxin steel plant (30.58° N, 118.1° E), Wan power plant (30.52° N, 117.46° E) and Shangfeng cement plant (30.48° N, 117.48° E) are equipped with well established commercial DOAS analyzers, measuring SO_2 emissions before and/or after the performance of desulfurization. The three factories provide different characteristic interfering gas types and concentration levels. Fuxin steel plant exhibits most interference from CO and CO_2, whereas interference in Wan power plant is mainly from CO and NO_x, and interference in Shangfeng cement plant is from H_2O, CO and CO_2. The CO in Fuxin steel plant, NO_x in Wan power plant and H_2O or CO_2 in Shangfeng cement plant are occasionally exhibit nonlinear absorptions. The accuracy level of all measurements can evaluate the performance of interference corrections within the multi-channel analyzer.

AMTD
8, 13331–13375, 2015

We carried out two field campaigns respectively in July 2011 and March 2012. The first campaign extended over three days from 6 to 8 July 2011, only operated in the Fuxin steel plant. The second campaign lasted ten days from 18 to 27 March 2012., sequentially operated in the Wan power plant and Shangfeng cement plant. The multi-channel analyzer was used to measure SO_2 emissions before the performance of desulfurization in both Fuxin steel plant and Wan power plant, while SO_2 emissions after desulfurization were measured in Shangfeng cement plant. All measurements were performed simultaneously with DOAS analyzers. The setup for the stack measurements is shown in Fig. 12. The pre-treated samples were pumped into the reference analyzer (a DOAS analyzer) and the multi-channel analyzer using a four-port distribution chamber. The pretreatment system was used to remove the dusts and liquids. The sample system blows back once an hour to prevent the dust filter from being jammed (this process called blowback). The multi-channel analyzer was zero and span calibrated before the experiments. Further details can be found in Sun et al. (2013).

Figure 13 shows SO_2 time series of Fuxin steel plant measured by a DOAS analyzer and the multi-channel analyzer on 6 July 2011. Measurements acquired during the blowback period are removed. The SO_2 measurements of the two analyzers exhibit very similar trends. SO_2 concentrations were throughout higher than 1000 ppmv and mainly concentrated between 1600 and 1800 ppmv. Figure 14 shows the corresponding correlation between the two analyzers after the outliers (measurements acquired during the blowback period) are removed. The correlation is quite good with $r^2 = 0.93218$.

Figure 15 shows SO_2 time series of Wan power plant measured by a DOAS analyzer and the multi-channel analyzer from 15:08 LT on 19 to 14:38 LT on 22 March 2012. Both analyzers acquired measurements once a minute, resulting in at least 4000 reliable measurements. For illustration here, the measurements acquired during blowback period are included, visible as outliers (sharp dips) in regular time intervals in Fig. 15. During the blowback period, gas samples pumped into the two analyzers are a mixture of emissions residuals and ambient air, causing measured concentrations to

AMTD
8, 13331–13375, 2015

drop down abruptly. The outliers measured by the DOAS analyzer appear sharper than those measured by the multi-channel analyzer, because the volume of the sample cell in the multi-channel analyzer is larger than that in the DOAS analyzer.

The trends of both concentration time series also agree well if outliers are discarded (outliers can easily be removed because blowback procedures are performed at fixed interval). SO_2 concentrations take values from 450 to 600 ppmv. Figure 16 shows the correlation between the two analyzers after the outliers are removed. A reasonable correlation with $r^2 = 0.86$ can be found for both types of measurement. The dense region within the green box represents SO_2 concentrations appearing with the highest frequency. Corresponding concentrations range from 450 to 600 ppmv.

Figure 17 finally shows the times series of hourly averaged SO_2 concentrations at Shangfeng cement plant measured by a DOAS analyzers and the multi-channel analyzer from 18 to 27 Mar 2012. The measurements acquired during blowback periods were again removed. Both analyzers show a very similar trend. SO_2 concentrations in most cases were less than 300 ppmv and mainly between 150 to 300 ppmv. Their correlation is illustrated in Fig. 18 ($r^2 = 0.89$). The green box has the same meaning as in Fig. 16. Concentrations range from 150 to 300 ppmv. From another continuous DOAS measurements we know that SO_2 concentrations of this factory before the desulfurization are usually around 600 to 900 ppmv, which are about three times the concentrations we measured during this field campaign.

It can be concluded from good agreements between the two analyzers at the three factories that the multi-channel analyzer is capable of monitoring SO_2 emissions in various industrial applications.

7 Conclusions

Industrial SO_2 emissions vary over a large range. They are embedded in exhausts comprised of a mixture of different gases which due to their interfering absorptions might affect measurements of SO_2 in the infrared spectral region. We design a multi-

AMTD
8, 13331–13375, 2015

channel gas analyzer with an optimized retrieval algorithm to solve these problems. The multi-channel gas analyzer measures the optical absorption of 11 wavelength channels simultaneously. We determine the filter parameters for all channels based on the measurement range requirements, a line-by-line (lbl) calculation method as well as an iterative scheme. Gaussian transmission functions for all filters are assumed. The influence of temperature and pressure on absorption line strengths and line shape functions are considered precisely in the data analysis. An optimized retrieval algorithm is developed to retrieve SO_2 concentration. It uses a 3rd polynomial rather than a constant factor to quantify gas-to-gas interference. The developed technique solved the linearity restriction of conventional interference correction of both intended and interfering channels. As a result, the interference correction can be extended to the nonlinear range. A good balance between sensitivity and measurement range was obtained, SO_2 concentrations ranging from ~5 to 10 000 ppmv can be detected with an excellent accuracy. Laboratorial and field experiments are performed to evaluate the performance of the developed retrieval algorithm within this multi-channel gas analyzer. The results show that the multi-channel gas analyzer is a robust solution for SO_2 emissions monitoring in industrial facilities. This measurement technique can potentially be applied to other gases measurements which feature with large concentration variation range, e.g. CO_2, H_2O, NO_2, etc.

Acknowledgements. This work is jointly supported by Anhui Province Natural Science Foundation of China (Grant NO. 1308085QF124) and the National Natural Science Foundation of China (Grants No. 41275037, No. 41275038 and No. 41575021). We thank Fuxin steel plant, Wan power plant and Shangfeng cement plant for access to the field sites. We would like to thank our colleague Y. Zhen for the source code of the Voigt profile calculation software which formed the basis of the total absorption coefficients calculation program in this study. We give many thanks to Andreas Hartl for his valuable comments and English improvements on the manuscript. The DOAS measurements are all provided by Landun environmental instrument, Inc.

AMTD
8, 13331–13375, 2015

References

Andre, G., Gerard, F., and Pierre, C.: Gas concentration measurement by spectral correlation: rejection of interfering species, Appl. Optics, 14, 2127–2132, 1985.

Bingham, D. and Burton, C. H.: Analysis of multi-component gas mixtures by correlation of infrared spectra, Appl. Spectrosc., 5, 705–709, 1984.

Bjorck, A.: Numerical Methods for Least Squares Problems, SIAM available at: http://www.ec-securehost.com/SIAM/ot51.html (last access: 2 March 2013), 1996.

Chan, C. K. and Yao, X.: Air pollution in mega cities in china, Atmos. Environ., 42, 1–42, 2008.

Dirk, A., Gaston, E. M., Shrikrishna, H. N., and Robert, F. M.: Gas Analyzer System, US Pat US/2009/0213380 A1, 27 August 2009.

Derek, Y.: Least squares fitting of a straight line with correlated errors, Earth Planet. Sc. Lett., 5, 320–324, 1968.

EPER: European Pollutant Emission Register 2004, http://www.eea.europa.eu/ (last access: 1 February 2012), 2004.

European Commission: 2007/589/EC, establishing guidelines for the monitoring and reporting of greenhouse gas emissions pursuant to Directive 2003/87/EC of the European Parliament and of the Council, Official Journal of the European Union, 2210, 2007.

Evans, S., Deery, S., and Bionda, J.: How Reliable are GHG Combustion Calculations and Emission Factors, Presented at the CEM 2009 Conference, 23–25 September 2009, Milan, Itlay, 2210, 2240, 2009.

Ehret, G., Kiemle, C., Renger, W., and Simmet, G.: Airborne remote sensing of tropospheric water vapor with a near infrared differential absorption lidar system, Appl. Optics, 24, 4534–4549, 1993.

Gary, K.: An open path H_2O/CO_2 gas analyzer for eddy correlation systems: theory and design, Spectrochim. Acta A, 58, 2373–2388, 2002.

Herget, W. F., Jahnke, J. A., Burch, D. E., and Gryvnak, D. A.: Infrared gas filter correlation instrument for in situ measurement of gaseous pollutant concentrations, Appl. Optics, 15, 1222–1225, 1976.

Harold, S. L., Satoru, S., Louis, J. D., and Alberto, M. G.: None-Dispersive Infrared Gas Analyzer with Interfering Correction, US Pat 5886348, 23 March 1999.

Jacob, Y. W. and Roy, L. A.: Non-dispersive infrared gas measurement, IFSA Publishing, 2, 4–69, 2012.

AMTD
8, 13331–13375, 2015

Komhyr, W. D., Waterman, L. S., and Taylor, W. R.: Semiautomatic non-dispersive infrared analyzer apparatus for CO_2 air sample analyses, J. Geophys. Res., 88, 1315–1322, doi:10.1029/JC088iC02p01315, 1983.

Komhyr, W. D., Harris, T. B., Waterman, L. S., Chin, J. F. S., and Thoning, K. W.: Atmospheric carbon dioxide at Mauna Loa Observatory: 1. NOAA global monitoring for climatic change measurements with a non-dispersive infrared analyzer, J. Geophys. Res.-Atmos., 94, 7–29, 1989.

Lambrecht, A.: Quantum cascade lasers, systems, and applications, in: Europe, Quantum Sensing and Nanophotonic Devices II, edited by: Razeghi, M., Brown, G. J., Proceedings of SPIE Vol. 5732, SPIE, Bellingham, WA, doi:10.1117/12.606470, 2–7 November 2005.

López, F. and de Frutos, J.: Multi-spectral interference filters and their application to the design of compact non-dispersive infrared gas analyzers for pollution control, Sensors and Actuators A: Physical, 37, 502–506, 1993.

Liu, C., Beirle, S., Butler, T., Liu, J., Hoor, P., Joeckel, P., Penning, V. M., Pozzer, A., Frankenberg, C., Lawrence, M. G., Lelieveld, J., Platt, U., and Wagner, T.: Application of SCIAMACHY and MOPITT CO total column measurements to evaluate model results over biomass burning regions and Eastern China, Atmos. Chem. Phys., 11, 6083–6114, 2012, http://www.atmos-chem-phys.net/11/6083/2012/.

Mauri, A. R., Llobat, M., and Adria, D.: Detection and correction of interferences in spectroscopy techniques, Anal. Chim. Acta, 426, 135–146, 2001.

Martin, K. and Michael, H.: Efficient line-by-line calculation of absorption coefficients, J. Quant. Spectrosc. Ra., 63, 97–114, 1999.

Mark, A. M., Chris, W. B., and Donald, S. L.: Nonlinear multi-component analysis by infrared spectrophotometry, Anal. Chem., 11, 1694–1703, 1983.

Marcel, M. and Zuberbuehler, A. D.: Nonlinear least-squares fitting of multivariate absorption data, Anal. Chem., 62, 2220–2224, 1990.

Rao, C. R., Toutenburg, H., Fieger, A., Heumann, C., Nittner, T., and Scheid, S.: Linear Models: Least Squares and Alternatives, Springer Series in Statistics, Springer-Verlag New York, Inc., New York, 1999.

Rothman, L., Jaquemart, D., Barbe, A., Benner, D. C., Birk, M., Brown, L., Carleer Jr, M. C. C., Chance, K., Coudert, L., Dana, V., Devi, V., Flaud, J.-M., Gamache, R., Goldman, A., Hartmann, J.-M., Jucks, K., Makim, A., Mandin, J.-Y., Massie, S., Orphalh, J., Perrin, A., Rinsland, C., Smith, M., Tennyson, J., Tolchenov, R., Toth, R., Auwera, J. V., Varanasi, P., and

AMTD
8, 13331–13375, 2015

Wagner, G.: The HITRAN 2004 molecular spectroscopic database, J. Quant. Spectrosc. Ra., 96, 139–204, doi:10.1016/j.jqsrt.2004.10.008, 2005.
Rothman, L., Gordon, I., Barbe, A., Benner, D., Bernath, P., Birk, M., Boudon, V., Brown, L., Campargue, A., Champion, J.-P., Chance, K., Coudert, L., Dana, V., Devi, V., Fally, S., Flaud, J.-M., Gamache, R., Goldman, A., Jacquemart, D., Kleiner, I., Lacome, N., Lafferty, W., Mandin, J.-Y., Massie, S., Mikhailenko, S., Miller, C., Moazzen-Ahmadi, N., Naumenko, O., Nikitin, A., Orphal, J., Perevalov, V., Perrin, A., Predoi-Cross, A., Rinsland, C., Rotger, M., Simeckova, M., Smith, M., Sung, K., Tashkun, S., Tennyson, J., Toth, R., Vandaele, A., and Auwera, J. V.: The HITRAN 2008 molecular spectroscopic database, J. Quant. Spectrosc. Ra., 110, 533–572, doi:10.1016/j.jqsrt.2009.02.013, 2009.
Sparks, L.: Efficient line-by-line calculation of absorption coefficients, J. Quant. Spectrosc. Ra., 57, 31–50, 1997.
Sayed, A. M. M. and Mohamed, H. A.: Gas analyzer for continuous monitoring of carbon dioxide in gas streams, Sensor. Actuator., 145, 398–404, 2010.
Miller, M. A. and Yuter, S. E.: Detection and characterization of heavy drizzle cells within subtropical marine stratocumulus using AMSR-E 89-GHz passive microwave measurements, Atmos. Meas. Tech., 6, 1–13, doi:10.5194/amt-6-1-2013, 2013.
Terje, B.: Impact of increased anthropogenic emission in Asia on troposphere ozone and climate, Tellus, 3, 251–254, 1996.
Tyson, L., Ling, Y. C., and Charles, K. M.: Simultaneous multi-component quantitative analysis by infrared absorption spectroscopy, Appl. Spectrosc., 5, 38–56, 1984.
Tan, Q. L., Zhang, W. D., Xue, C. Y., Xiong, J. J., Ma, Y. C., and Wen, F.: Design of mini-multi-gas monitoring system based on IR absorption, Opt. Laser. Technol., 40, 703–710, 2008.
Zu, S. F.: Present status and developing countermeasure of tail exhaust gas measurement of China motor vehicle, Auto. Ind. Res., 4, 25–28, 2002.

AMTD
8, 13331–13375, 2015

Table 1. Filter parameters: center wavelengths, bandwidths and transmissions. The bandwidths of Ref, SO_2(L) and SO_2(H) filters are calculated using the iterative scheme described in the text. The transmissions of all filters are approximated by Gaussian functions with maximum transmission of 75 %.

Channel (#)	#0	#2	#3
Filters	Ref [a]	SO_2(L) [b]	SO_2(H) [c]
Center wavelength (μm)	3.73	7.32	4.00
bandwidth (μm)	0.08	0.4	0.1
Transmission (%)	75	75	75

[a] Reference filter channel.
[b] Filter channel used to measure SO_2 for low concentration levels.
[c] Filter channel used to measure SO_2 for high concentration levels.

AMTD
8, 13331–13375, 2015

Table 2. Total absorption coefficients, lower and top detection limits of Ref, SO_2(L) and SO_2(H) calculated using the parameters in Table 1.

Channel (#)	Wavelength intervals (μm)	Total absorption coefficients (cm^2 $molecule^{-1}$)	Lower detection limits (ppmv)	Top detection limits (ppmv)
Ref	3.65–3.81	2.46113×10^{-23}	88270.9	5.15537×10^{6}
SO_2(L)	6.92–7.72	4.04201×10^{-19}	5.3747	313.904
SO_2(H)	3.9–4.1	8.91975×10^{-21}	243.556	14224.6

AMTD
8, 13331–13375, 2015

Table 3. The nomenclature in Fig. 3.

items	nomenclature	items	nomenclature
#1–10	H_2O, SO_2(L), SO_2(H), NO, NO_2, CO, CO_2, N_2O, CH_4 and HC channels, respectively	τ_t'' (t = 2–10)	the cross interference corrected absorbance of channel #t.
τ_t(t = 1–10)	drift compensated absorbance of channel #t	$k_{t1}(x)$(t = 2–10)	the interference function of H_2O to channel #t
τ_t'(t = 2–10)	water vapor interference corrected absorbance of channel #t	$k_{ij}(x)(i, j = 2–10$ and $i \neq j)$	the interference function of gas j to channel #i

AMTD
8, 13331–13375, 2015

Table 4. Statistical results for the absorbance time series in Fig. 6, the corresponding estimation results for measurement range are also included. Ten measurement cycles are averaged, resulting in a temporal resolution of about four seconds per reading.

Channel (#)	Sample number	Mean (-)[a]	1σ Standard deviation (-)	Maximum (-)	Minimum (-)	LDL[b] (ppmv)	TDL[c] (ppmv)
SO_2(L)	8275	-5.76798×10^{-7}	7.59723×10^{-6}	0.00209	-0.00324	5.54768	997.23
SO_2(H)	8275	2.98175×10^{-4}	8.90672×10^{-4}	0.00306	-0.00397	102.14842	26 059.02

[a] Absorbance; [b] Lower detection limit; [c] Top detection limit.

AMTD
8, 13331–13375, 2015

Table 5. SO_2 measurement results and corresponding measurement errors, Gas mixtures (H_2O, CO_2, CO, NO_x and SO_2) with 15 spans of SO_2 are measured in sequence, five and ten spans of these gases lie within the measurement range of SO_2 (L) and SO_2 (H) channel, respectively.

No.	True concentration (ppmv)	Measurement concentration (ppmv)	Measurement biases par $\lvert\Delta C\rvert$ (ppmv)	Relative measurement errors (%)
0	0	1.3	1.3	1.3
1	86	84.1	1.9	2.2
2	132	134.3	2.3	1.7
3	187	184.4	3.6	1.9
4	243	238.6	4.4	1.8
5	356	363.5	7.5	2.1
6	855	866.1	11.1	1.3
7	1623	1600.3	22.7	1.4
8	2884	2921.5	37.5	1.3
9	3667	3711	44	1.2
10	4543	4492	51	1.13
11	5758	5700.4	57.6	1.0
12	6672	6598.6	73.4	1.1
13	7376	7454.2	78.2	1.06
14	8688	8775.7	87.7	1.01

AMTD
8, 13331–13375, 2015

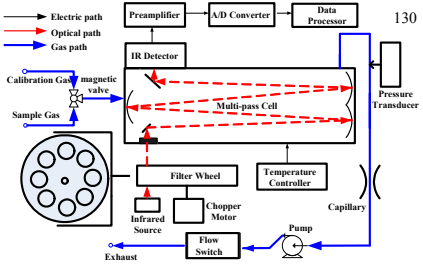

(a) functional structure

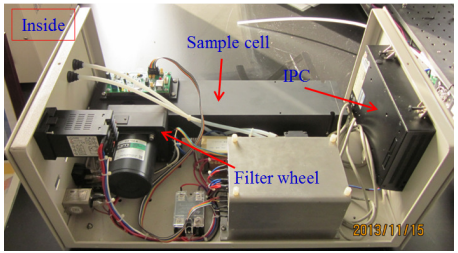

(b) inside view

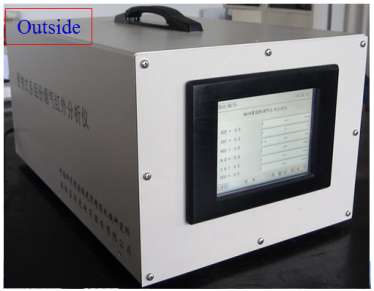

(c) outside view

Figure 1. Layout of the experimental setup, **(a)** functional structure and **(b)** outside view.

AMTD
8, 13331–13375, 2015

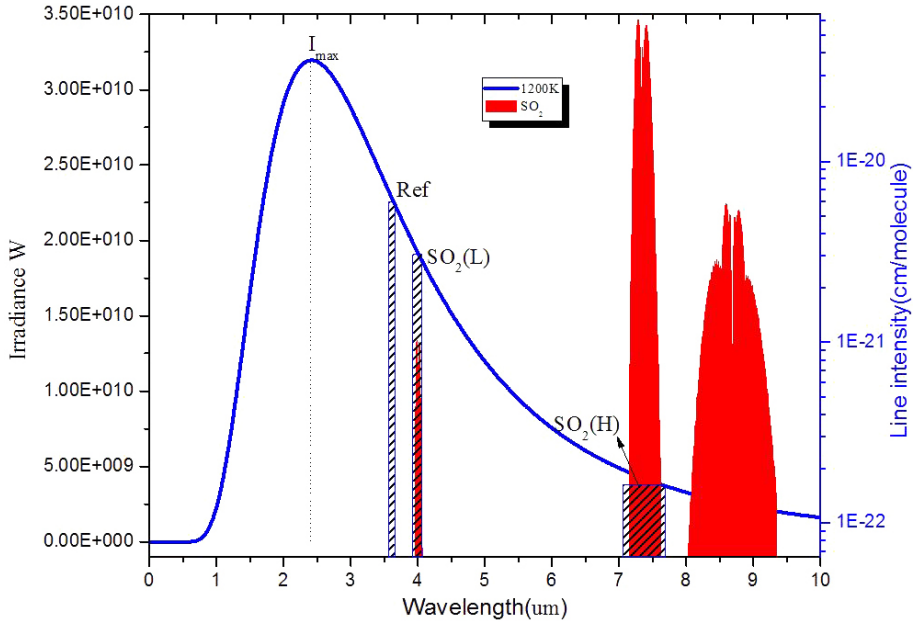

Figure 2. Overview of the radiation distribution of the light source, the bandwidths of Ref, SO_2 (L) and SO_2 (H) filters and the absorption spectra of SO_2 between 2 and 10 µm obtained from the HITRAN database. The curves are in linear-log plots and three obvious absorption wavebands at 4, 7.32 and 8.5 µm are shown. Their line strengths ranked as 7.32 µm > 8.5 µm > 4 µm with values 10^{-19}, 10^{-20} and 10^{-21} cm/molecule, respectively.

AMTD
8, 13331–13375, 2015

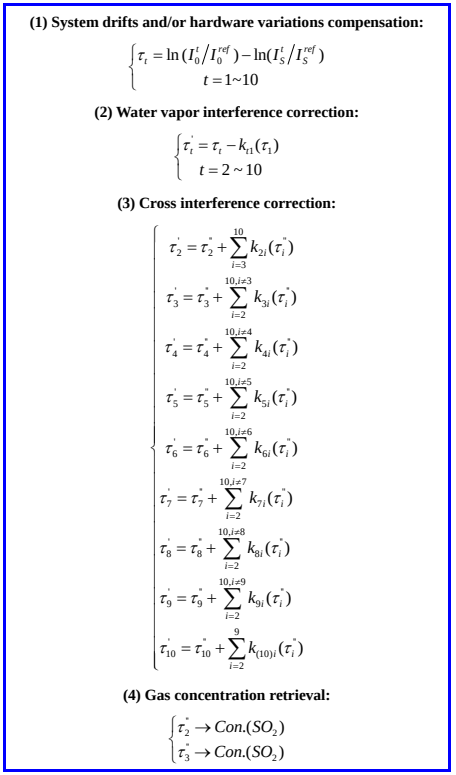

Figure 3. Concentration retrieval consisting of the four steps shown. The instrument measures intensities of all channels. Measurement values are converted into absorbance and corrected for water vapor interference using the water vapor channel. Cross interference corrections are performed using interference equations. Corrected absorbance are finally converted into SO_2 concentrations. See text for further details.

AMTD
8, 13331–13375, 2015

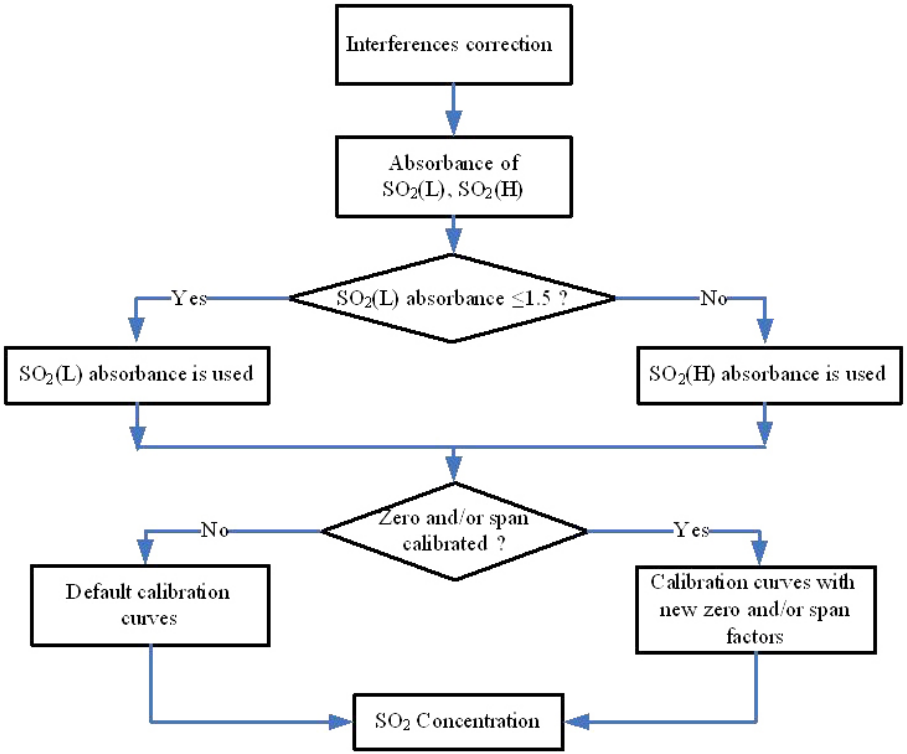

Figure 4. Flow chart of SO_2 concentration retrieval. The retrieval channel is chosen based on the interference corrected absorbance of SO_2 (L). See text for further details.

AMTD
8, 13331–13375, 2015

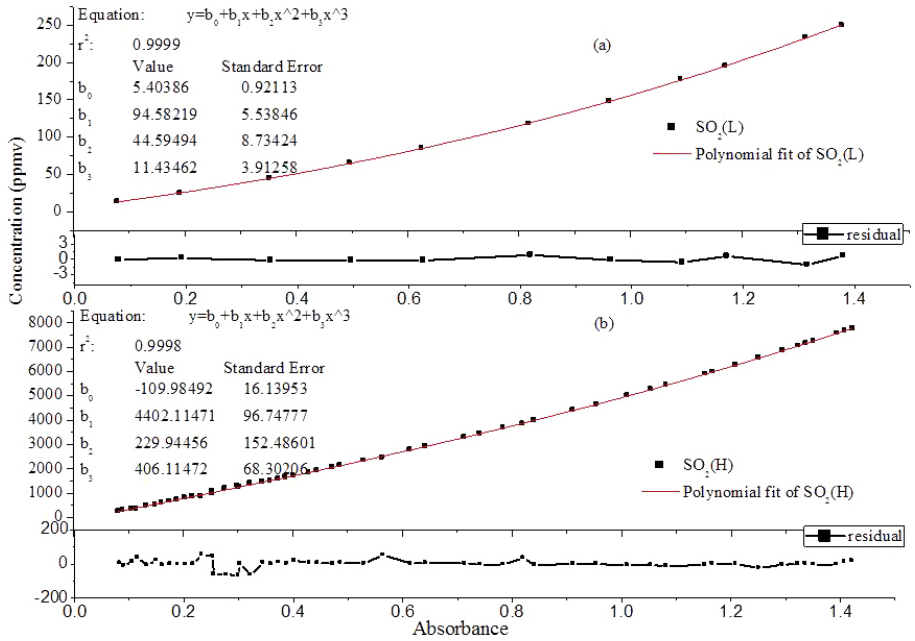

Figure 5. Calibration curves for SO_2 (L) **(a)** and SO_2 (H) **(b)** as result of a least-squares fitting using a 3rd order polynomial model.

AMTD
8, 13331–13375, 2015

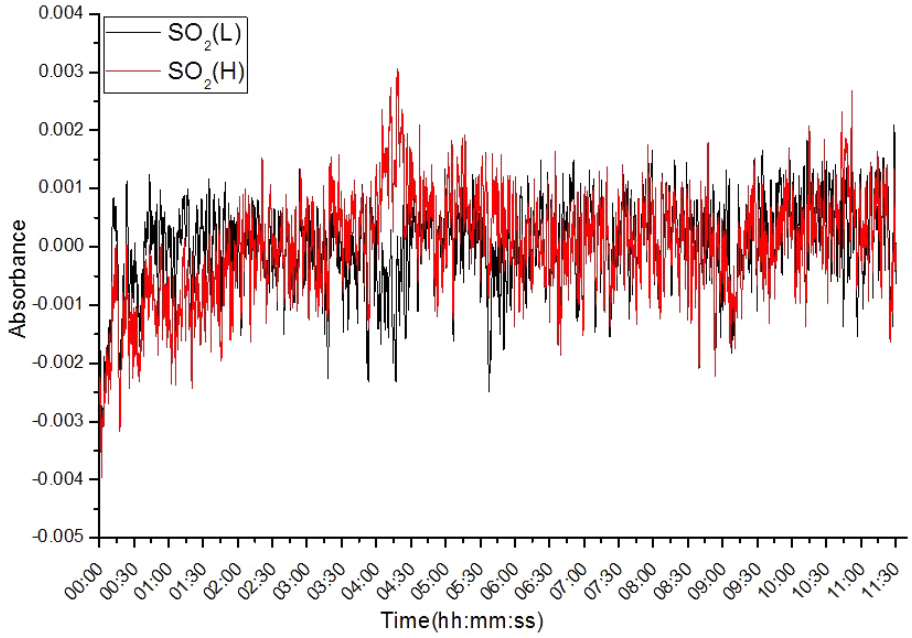

Figure 6. Absorbance time series for the SO_2 (L) and SO_2 (H) channel under zero gas (99.999 % N_2) condition. Sample data more than 10 h are included.

AMTD
8, 13331–13375, 2015

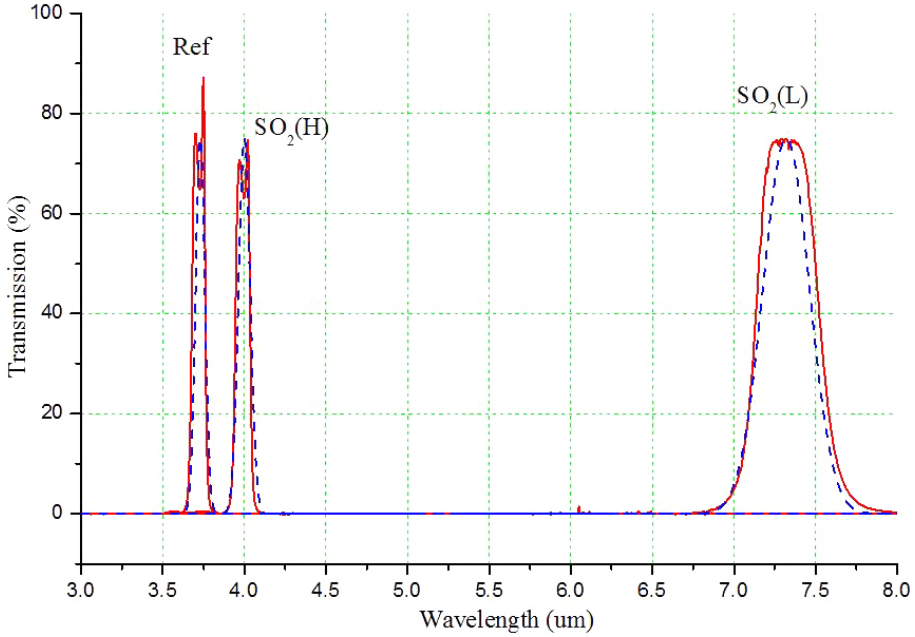

Figure 7. Transmissions of the filters in Table 1. The red solid lines are actual transmission functions and the blue dotted lines are corresponding Gaussian functions assumed in Sect. 3.

AMTD
8, 13331–13375, 2015

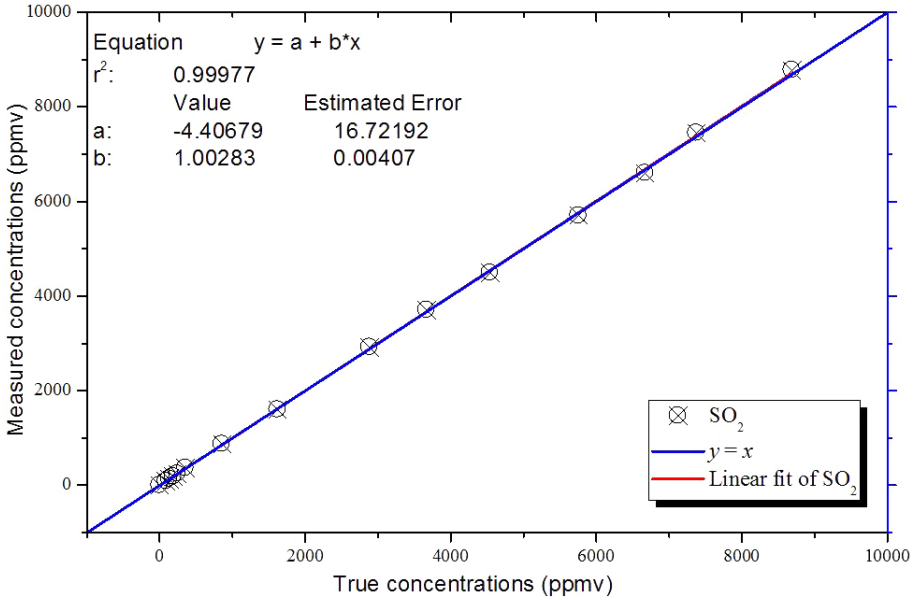

Figure 8. Linear correlation between retrieved and true concentrations. An excellent Pearson correlation coefficient r^2 of 0.99977 is obtained.

AMTD
8, 13331–13375, 2015

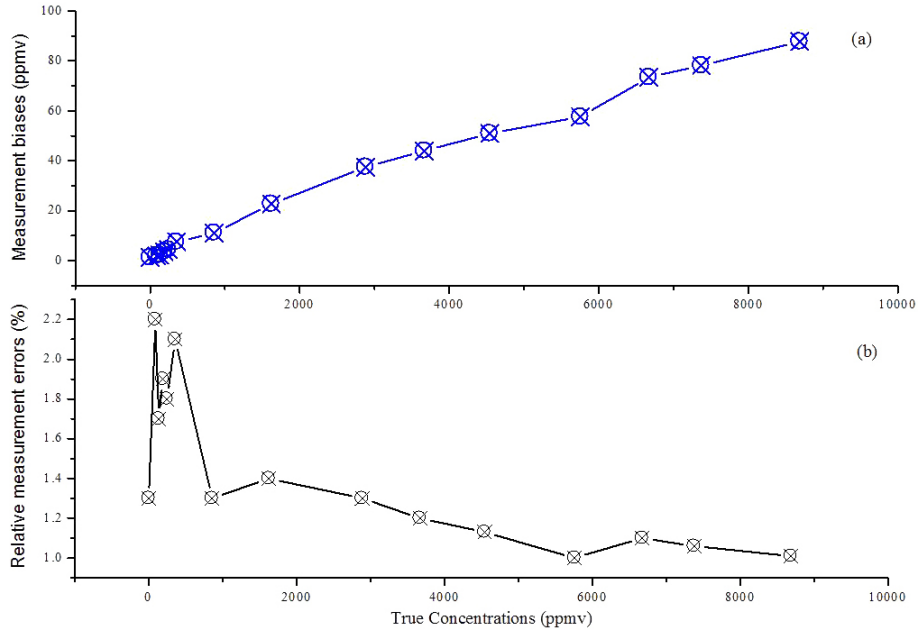

Figure 9. Comparison of measurement bias **(a)** and relative measurement errors **(b)** for all concentration spans of the laboratory experiment. The measurement bias obviously increases with increasing concentrations. Relative measurement errors for high concentrations are smaller than those for low concentrations.

AMTD
8, 13331–13375, 2015

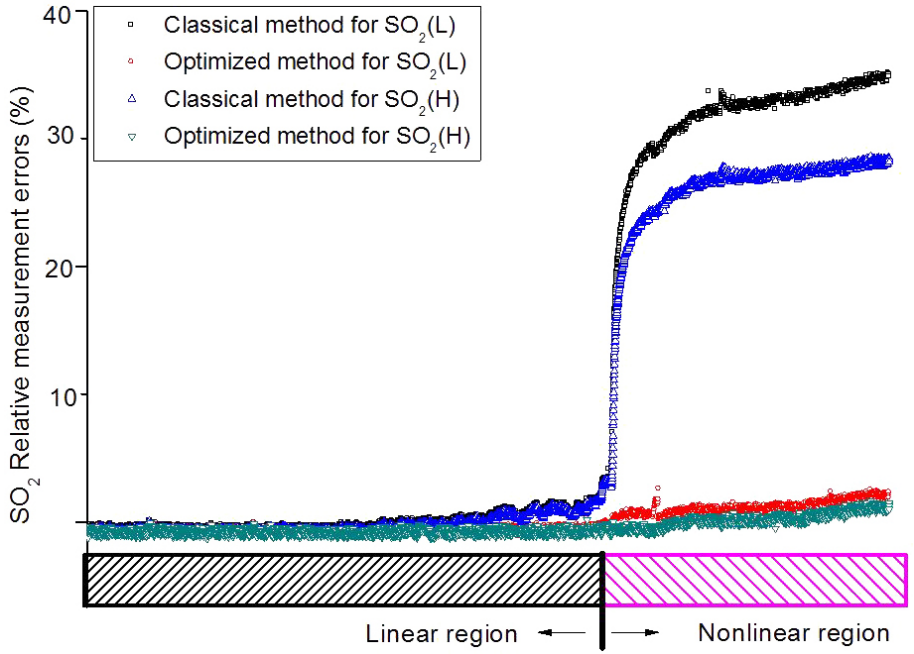

Figure 10. Comparison between the conventional and the optimized retrieval algorithm. H_2O absorption varied gradually from linear region to nonlinear region.

AMTD
8, 13331–13375, 2015

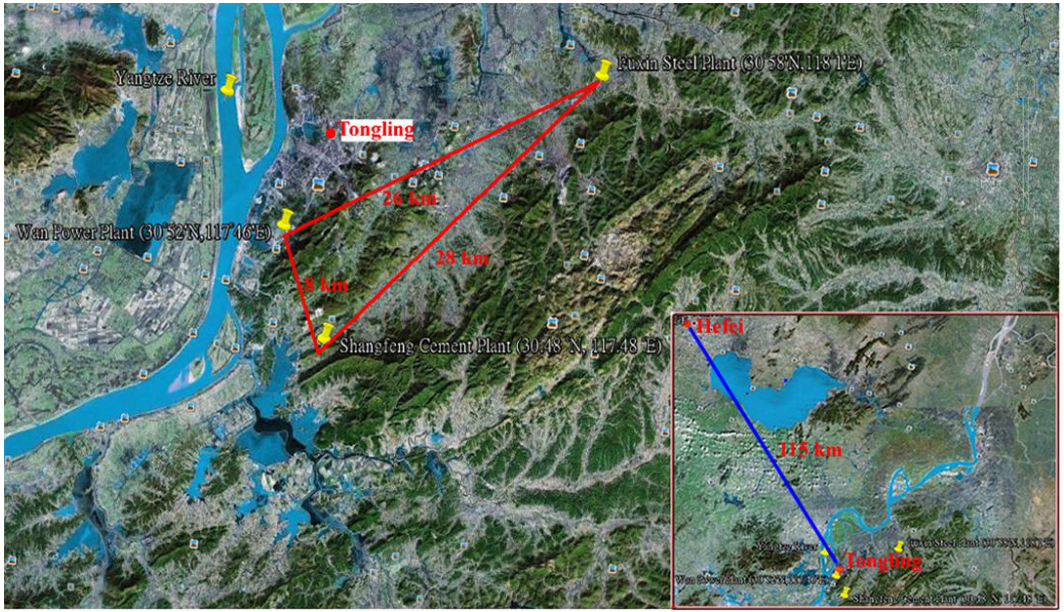

Figure 11. The location of the Fuxin steel plant (30.58° N, 118.1° E), the Wan power plant (30.52° N, 117.46° E) and the Shangfeng cement plant (30.48° N, 117.48° E). The three factories form a triangle near the Yangtze River, and all are located in the suburbs of Tongling city (south of Hefei, Anhui province) in central China.

AMTD
8, 13331–13375, 2015

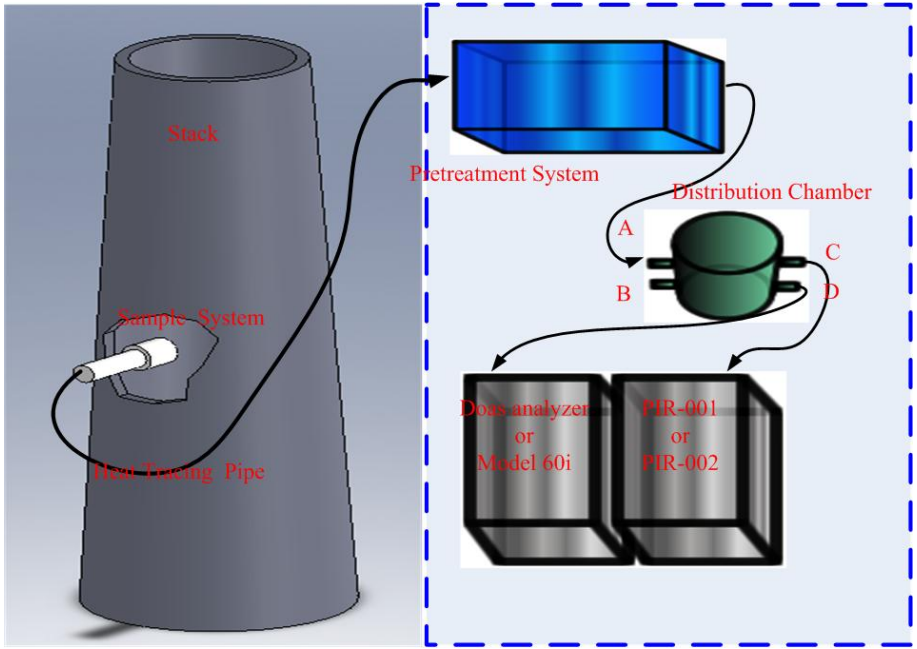

Figure 12. Setup for stack measurements with the multi-channel analyzer and a DOAS analyzer. A detailed description of a similar setup can be found in Sun et al. (2013).

AMTD
8, 13331–13375, 2015

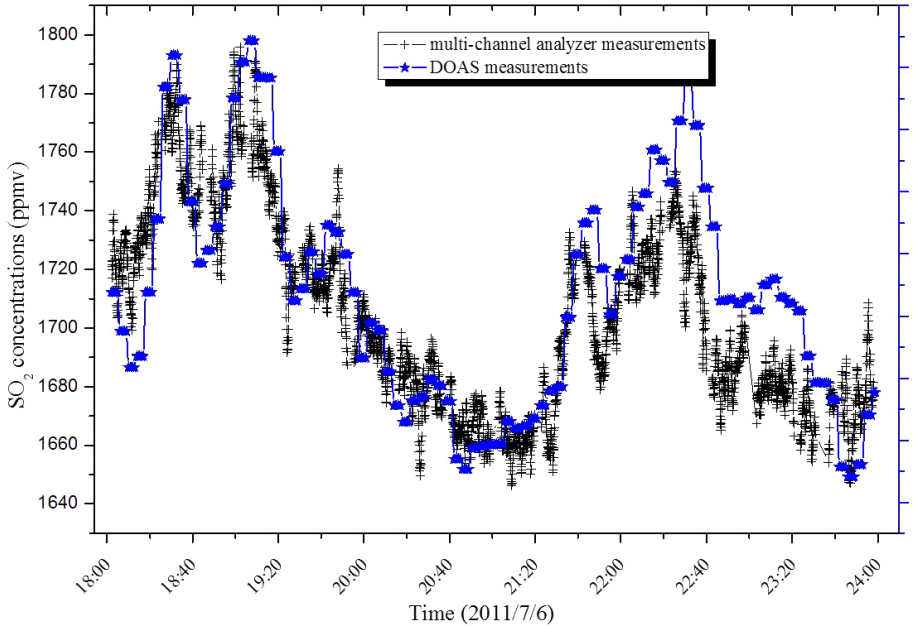

Figure 13. SO_2 concentration series of Fuxin steel plant measured by a DOAS analyzer and the multi-channel analyzer on 6 July 2011. Measurements acquired during blowback period are removed.

AMTD
8, 13331–13375, 2015

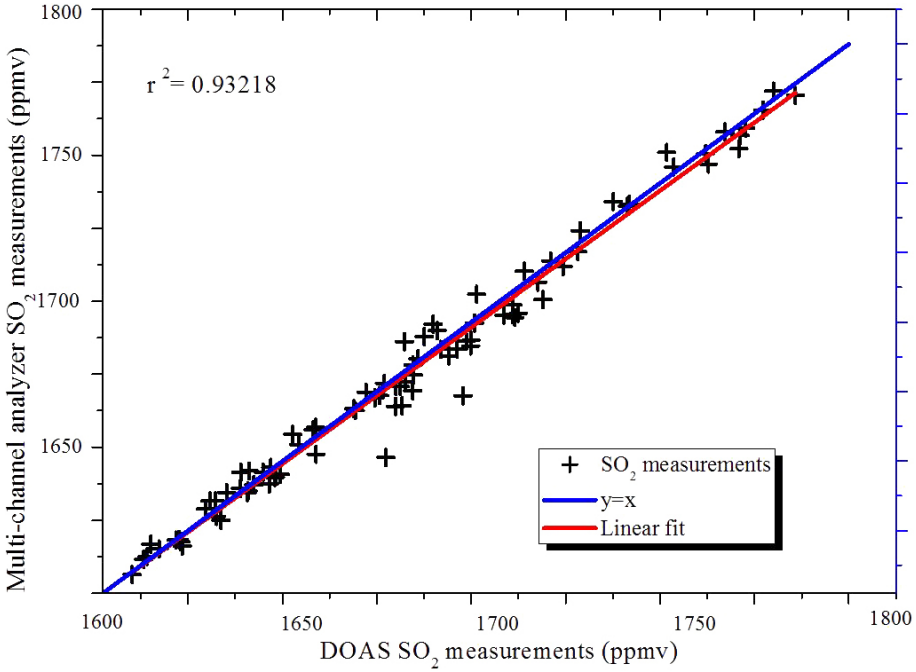

Figure 14. Correlation between SO_2 concentrations measured by a DOAS analyzer and the multi-channel analyzer on 6 July 2012 at the Fuxin steel plant (Outliers during the blowback period are removed).

AMTD
8, 13331–13375, 2015

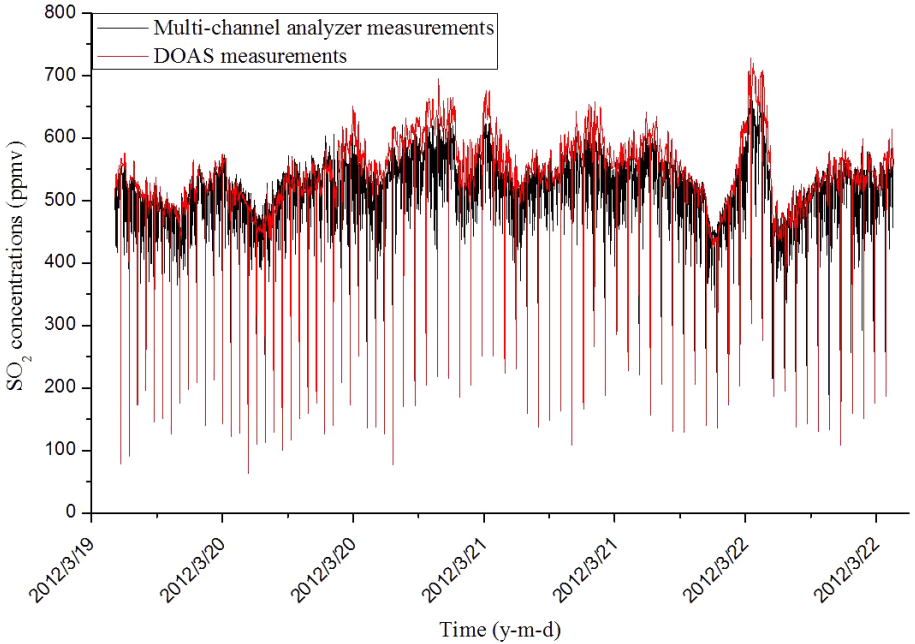

Figure 15. SO_2 concentrations time series of Wan power plant measured by a DOAS analyzer and the multi-channel analyzer during 18 to 27 March 2012. Measurements acquired during blowback periods are included, appearing as sharp drop downs of the concentration at fix intervals.

AMTD
8, 13331–13375, 2015

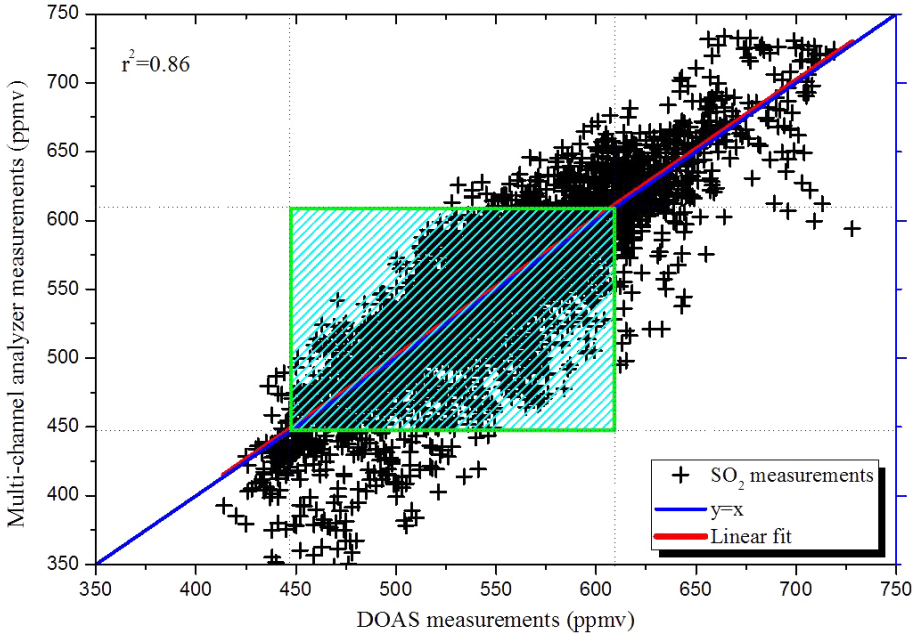

Figure 16. Correlation between a DOAS analyzer and the multi-channel analyzer for the time series shown in Fig. 15 after outliers were removed. The green box represents SO_2 concentrations that appeared with the highest frequency.

AMTD
8, 13331–13375, 2015

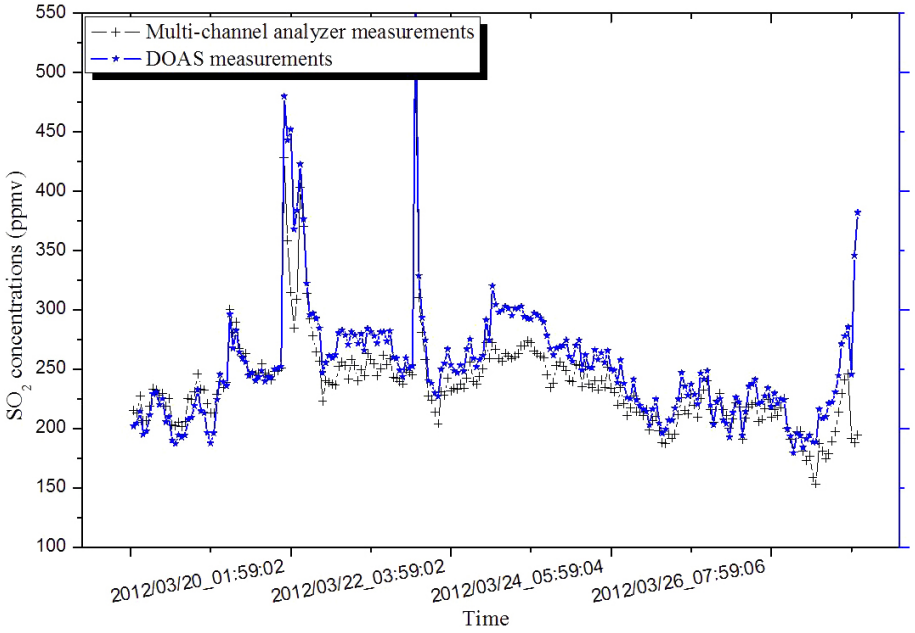

Figure 17. Time series of hourly averaged SO_2 concentrations measured by the DOAS analyzer and the instrument introduced in this work at the Shangfeng cement plant. Measurements acquired during blowback periods were removed.

AMTD
8, 13331–13375, 2015

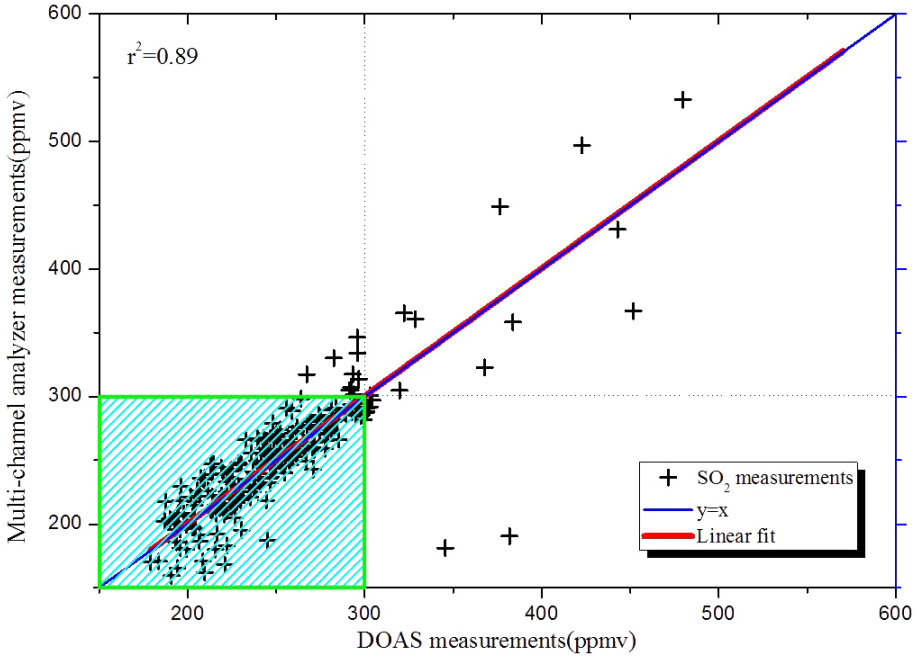

Figure 18. Correlation between the two analyzers for the time series of Fig. 17. The green box again represents SO_2 concentrations appearing with the highest frequency.

AMTD
8, 13331–13375, 2015